Bulletin of the Seismological Society of America, Vol. 97, No. 1A, pp. S208–S222, January 2007, doi: 10.1785/0120050611

Numerical Modeling of the Great 2004 Indian Ocean Tsunami: Focus on the Mascarene Islands

by H. Hébert, A. Sladen, and F. Schindelé

Abstract On 26 December 2004, the M_w 9.2 Sumatra earthquake triggered the greatest tsunami ever observed in recent times. The unprecedented quality and variety of observations on modern instruments provide opportunities to refine modeling techniques as well as our perception of tsunami hazard in oceanic regions where historical events are not as frequent as in the Pacific Ocean. We present a numerical modeling of the 2004 tsunami on the Mascarene Islands with refined computations on La Réunion Island, where postevent survey observations and one tide gauge record are available. We use two different source models (models A and B) to account for the observations, and we also test an additional source model (model C) to study the effect of a tsunami originating in the 1833 epicentral area (southern Sumatra). A wave trapped on the edge of La Réunion may explain the greatest water heights reached in the western coastline of the island. The observed tide gauge data are reasonably well fit (models A and B). The run-up data can also be explained with our models. Late disturbances observed in La Pointe des Galets may be explained by a late tsunami reflection from Madagascar or by harbor resonances. Finally we also show that model C (1833-like) strikes La Réunion more heavily than models A and B.

Introduction and Objectives

The size of the great M_w 9.2 Sumatra–Andaman earthquake (e.g., Lay *et al.*, 2005; Stein and Okal, 2005; Subarya *et al.*, 2006) was unexpected not only by geophysicists working on subduction zones and megathrust earthquakes, but also by tsunami researchers (Titov *et al.*, 2005). Indeed over recent centuries most of the destructive tsunamis triggered by megathrust earthquakes have occurred in the Pacific Ocean, where well-identified seismic gaps are now currently scrutinized as likely sources for large transoceanic tsunamis comparable to the 1946 (Aleutian) or 1960 (Southern Chile) events. One such gap is located in northern Chile that has not ruptured since 1877 (Delouis *et al.*, 1997; Chlieh *et al.*, 2004). The Sumatra–Andaman event nucleated in a gap region devoid of major seismic ruptures since 1861 or 1881 (Newcomb and McCann, 1987; Ortiz and Bilham, 2003; Chlieh *et al.*, 2007). Because the periods for such great Indian Ocean events appear to be longer that those for the Pacific Ocean, and few tsunamigenic events have occurred there in the twentieth century, the awareness of the tsunami risk in the region was obviously rather low, in the near field as well as farther in the Indian Ocean.

The 2004 event provides us with a huge amount of tsunami records on a wide variety of instruments and sensors, including conventional coastal tide gauges (Merrifield *et al.*, 2005; Rabinovich and Thomson, 2007), outstanding altimetry (Gower, 2005), infrasound (Le Pichon *et al.*, 2005), and hydroacoustic (Guilbert *et al.*, 2005; Hanson and Bowman, 2005; Hanson *et al.*, 2007) observations. All these data contribute to a large and growing database of gauges and run-up observations gathered not only from the Indian Ocean, but also in other oceanic basins including the Atlantic and Pacific oceans (Titov *et al.*, 2005). All these observational elements facilitate analyses and modeling of the 2004 event in much more detail than for earlier tsunami events.

Now we have the opportunity to test initiation, propagation, and run-up numerical modeling methods, to fit the gauges and run-up data, in the near or far field, and also to recover the source processes thanks to tsunami data (e.g., Sladen and Hébert, 2005; Fujii and Satake, 2007; Piatanesi and Lorito, 2007). In this article we focus on the far-field impact of the 2004 tsunami, namely on the Mascarene Islands, and especially La Réunion Island, which were struck by the waves about 7 hours after the earthquake (Fig. 1). We first present the available observations and then discuss the results of modeling. This allows an analysis of the reported sea-wave amplitudes and run-up heights, as well as a discussion of the amplification behavior of the harbor basins reported several hours after the first arrivals. Our aim is to discuss tsunami characteristics rather than earthquake-source details, but we also study the impact of choosing

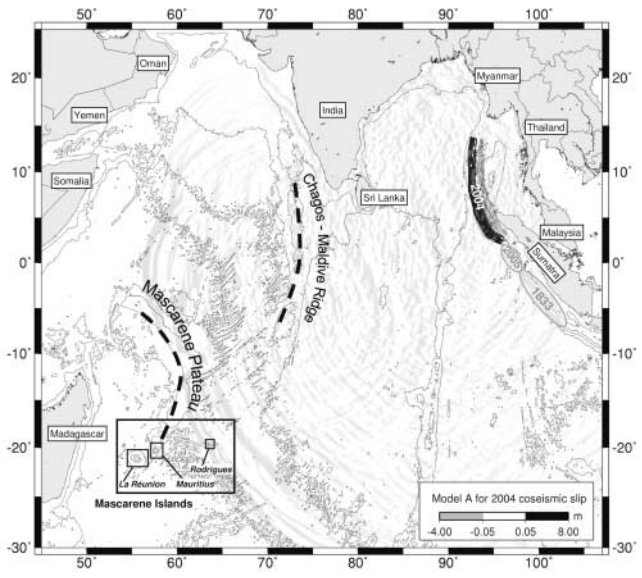

Figure 1. Regional setting of the 2004 Indian Ocean tsunami. Along the Andaman–Sumatra subduction, one source used for far-field modeling (model A) is displayed. The shadowed tsunami wave field computed with this model is displayed after 6 hours of propagation, when approaching the Mascarene Islands. Bathymetric contour interval is 2000 m.

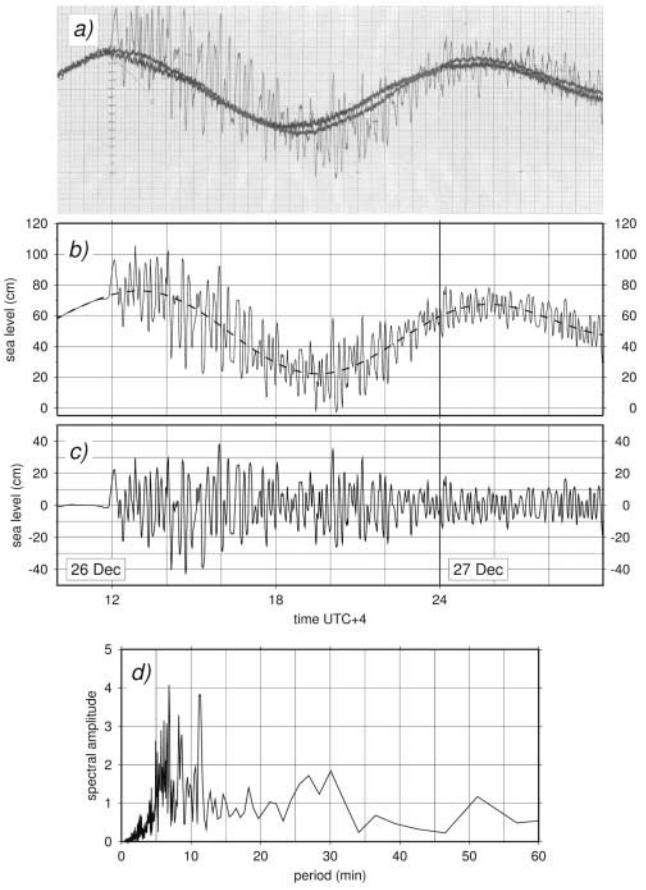

Figure 2. Tide gauge record in La Pointe des Galets (location of the gauge on Fig. 3). (a) Original record containing 3 days of superimposed recording. (b) Digitized, 30-sec sampled signal (solid line) and Fourier polynomial used to model the tidal signal (dashed line). (c) Residual tsunami signal. (d) Fourier transform of the residual signal.

different sources, to test the role of source heterogeneities and to try a southward, 1833-like source.

Observations of the Tsunami in La Réunion

Setting of the Mascarene Islands

The Mascarene Islands (Mauritius, Rodrigues, and La Réunion) are volcanic islands created since 10 Ma during the drift of the African plate over the Réunion hotspot, forming with the Mascarene Plateau and the Chagos-Maldives Ridge one of the major hotspot systems in the global ocean (Duncan, 1981; Morgan, 1981) (Fig. 1). La Réunion Island is a French overseas department characterized by an inactive volcano Piton des Neiges, and a continuously active volcano Piton de la Fournaise. The island is not protected by a developed coral reef or a lagoon, except on the coast south to Saint-Gilles in an area not exceeding a few kilometers long and a few hundreds of meters wide. The 2004 tsunami is the first event of this type in modern times and in this ocean, and it provides elements to study the response of a remote island to a major, modern transoceanic tsunami, to be compared with similar but older events that struck Hawaii or French Polynesia during the last century.

Tide Gauge Data

The tsunami waves were recorded on an analog OTT R16 tide gauge (Fig. 2) located in the western harbor of La Pointe des Galets (Fig. 3). These data are a good illustration of data recorded on an instrument not designed for tsunami recording, hence, far less designed for alert, with tidal waves continuously plotted but superimposed in phase for 3 days (Fig. 2a). The arrival of the tsunami, though well identified, is thus mixed with the tidal signal of the two previous days, which was graphically erased to recover the tsunami signal that was subsequently digitized (Fig. 2b). The tsunami arrival can be estimated to 11 h 45 m local time (UTC + 4) in good agreement with raytracing methods that predict a travel time slightly smaller than 7 hours (Titov *et al.*, 2005).

At first sight we observe that the tsunami perturbations lasted for at least 20 hr and that the sea level variations did not return to the basic noise level before the beginning of 27 December. The amplitudes corrected for the tidal signal reach 50 cm for at least 10 hr (Fig. 2c) and seem to correspond rather well to a complete signal, although some peaks (the 5th, 9th, an 11th peaks, between 12 h and 14 h) have been clipped by 5 cm at most, as remarked on the original paper record. The signal maintains a sustained am-

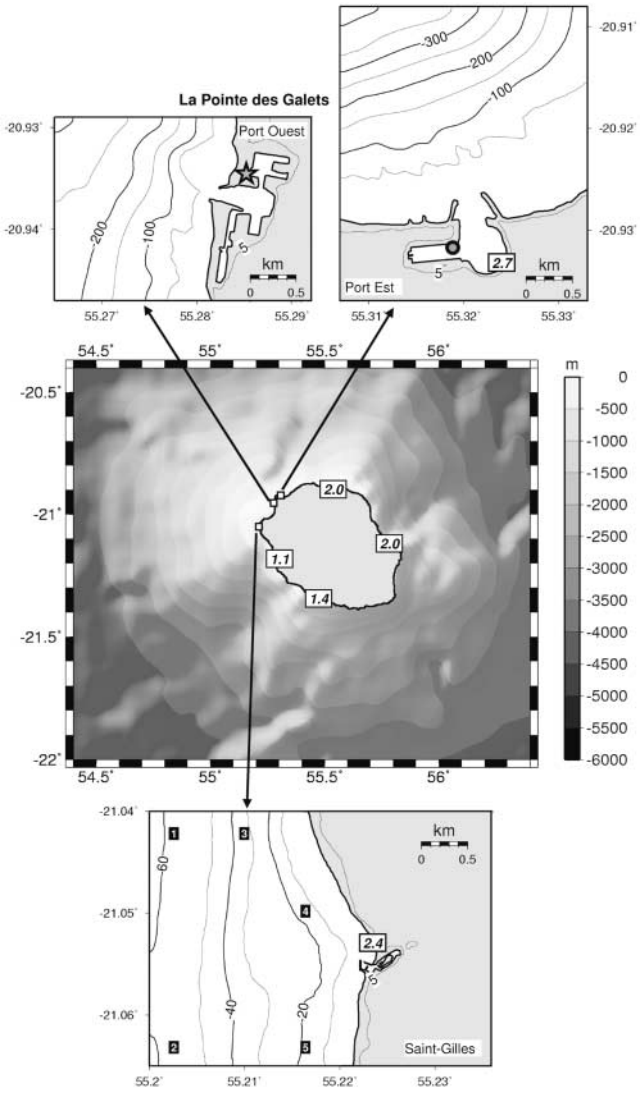

Figure 3. Setting of La Réunion Island. The 2004 run-up observations are displayed (italic numbers), with a maximum 2.7 m observed in the eastern basin of La Pointe des Galets (top right). The tide gauge location is noted with a star (top left), and location of the container ship displacement on 26 December 2004 is shown with a circle (top right). Synthetic tide gauges displayed on Figure 12 are also shown (white numbers in black squares).

plitude of 20 cm during the following 10 hours. Periods that can be identified range from 5 to 30 min (Fig. 2d), with a significant energy for periods of 25 to 30 min. These may correspond to the periods of the source, while higher energy in 5- to 10-min periods may illustrate local harbor resonances.

Postevent Survey

The tide gauge data are informative but primarily reflect a local response to the tsunami waves: they may underestimate the real and full impact of the tsunami, all the more since this harbor was not struck too severely. Indeed several locations around La Réunion were more damaged, as revealed by the postevent survey organized in March 2005 in the Mascarene Islands (Okal *et al.*, 2006c). The most affected island was Rodrigues, where several places were significantly flooded and maximum run-up reached 2.9 m. Effects in Mauritius were reported as very minor. The tsunami arrival in La Réunion was hardly noticed although local harbor facilities experienced substantial damage, especially on the western (La Pointe des Galets, Saint-Gilles; see Fig. 3) and northeastern (Sainte-Marie) coasts. While run-up data range from 1 to 2 m along the shoreline, a maximum 2.7-m run-up height was measured in the eastern basin of La Pointe des Galets.

In the La Pointe des Galets harbor, a container ship broke her moorings between 15 h 30 m and 15 h 45 m local time, thus about 10 h 30 m after the earthquake and more than 3 h after the first arrivals. Surprisingly, the same ship was remoored and again broke her moorings at 18 h 20 m, thus more than 13 h after the earthquake (Okal *et al.*, 2006c). The Indian Ocean tsunami seems to have provoked these types of late harbor disturbances at several remove locations, such as in Madagascar and Oman in addition to La Réunion (Okal *et al.*, 2006a, 2006b). Such inconveniences in harbors underline the long-lasting effect of the tsunami waves, possibly due to delayed dispersed wave trains or to particular oceanic behaviors such as reflections and scatterings, and stress the necessity for warning issuances to be held several hours after the first arrivals.

Methods

Tsunami Modeling

Tsunami modeling is carried out using the classical, nonlinear shallow-water theory, that proved efficient to assess tsunami hazard in French Polynesia or to study historical events (Heinrich *et al.*, 1998; Hébert *et al.*, 2001, 2005). This method accounts for nonlinear processes in coastal areas contrary to similar linear methods that remain valid in the deep ocean (e.g., Fujii and Satake, 2007; Piatanesi and Lorito, 2007). The source is treated as an instantaneous perturbation of the seabottom in response to the static displacement due to the earthquake. The initial deformation is computed through a model of elastic dislocation (Okada, 1985) constrained with seismological parameters of the rupture that satisfy the expression of moment magnitude $M_0 = \mu ULW$, where μ is the rigidity, U is the average slip amount, and L (W) is the length (width) of the fault plane (e.g., Kanamori and Anderson, 1975). The total initial displacement provides the initial condition to solve the hydrodynamic equations:

$$\frac{\partial(\eta + h)}{\partial t} + \nabla \cdot [(\mathbf{v}(\eta + h)] = 0 \qquad (1)$$

$$\frac{\partial(\mathbf{v})}{\partial t} + (\mathbf{v} \cdot \nabla)\mathbf{v} = -\mathbf{g}\nabla\eta, \qquad (2)$$

where h is the sea depth, η is the water elevation above mean sea level, **v** is the depth-averaged horizontal velocity vector, and **g** is the gravitational acceleration.

Equations of continuity (1) and motion (2) are solved in spherical coordinates by means of a finite-difference method, centered in time, and with use of an upwind scheme in space. Under the shallow-water theory dispersive effects are neglected. The phase velocity $c = (gh)^{1/2}$ drastically decreases close to the coasts where the shoaling effect leads to wave amplification. The decreasing tsunami wavelength near the shoreline requires finer bathymetric grids. To properly model the tsunami arrival at the local scale we use a series of five levels of nested bathymetric grids characterized by an increasing resolution, from 2′ (3.7 km) in deep ocean down to 15 m in the harbors, and the stability is ensured by using a decreasing timestep. Open free-boundary conditions are ascribed to the boundaries of the larger and coarser grid, and wave heights and velocities along the boundaries of a fine grid are spatially interpolated at each timestep from the values computed in the coarse grid containing the fine grid.

Bathymetric and Topographic Data

The large grid covering the Indian Ocean has been extracted from ETOPO2 bathymetric data derived from satellite altimetry (Smith and Sandwell, 1997). Successive interpolations allowed the building of nested bathymetric grids down to the island scale where hydrographic maps 7035 (scale 1/750,000) and 7183 (scale 1/60,000) from the French Hydrographic Service SHOM (Service Hydrographique et Océanographique de la Marine) have been gradually integrated to improve the resolution for coastal grids. In each studied harbor basin (map subset at scale 1/10,000), contour levels at 10-m intervals and isolated benchmarks have been digitized and interpolated to build the 15-m grids describing both basins of La Pointe des Galets and Saint-Gilles (Fig. 3). We did not use any modern multibeam data available in the area for our computations, though they would be of higher quality. For the scope of the present study, hydrographic maps were easily available and presented the advantage of providing bathymetric values up to the shallowest, coastal domains, including harbor basins.

Finally topographic data from the topographic map 4401RT from IGN (Institut Géographique National, scale 1/25,000) have been added to compute run-up. Unfortunately no contour level lower than 10 m was available; therefore, the quality of the topographic data, hence of the computed run-up, essentially depends on the interpolation carried out between the shoreline and the 10-m contour locally improved with few topographic benchmarks and information made by the survey team (Okal *et al.*, 2006c). The interpolated 5-m topographic contour is thereby shown on Figure 3. So far, sensitivity analysis has not been carried out to assess the run-up quality as a function of topographic uncertainty, a matter that could be examined when high-quality topographic data in the range 0–5 m are available. Accordingly the results are discussed relatively with respect to the different source models used.

The obtained bathymetric grids describing the studied sites exhibit some contrasting features (Fig. 3). The harbor of Saint-Gilles is characterized by a shallow submarine shelf that extends offshore down to the 60-m bathymetric contour level, whereas in both other basins (La Pointe des Galets) the 300-m bathymetric contour level is reached at almost the same 2-km horizontal offshore distance. This implies that the submarine slopes off Saint-Gilles are almost five times less steep than the submarine slopes off La Pointe des Galets, and besides the 7183 SHOM map also reveals that at Saint-Gilles the shallow area (less than 100 m deep) extends at least 4 km offshore. These features theoretically favor tsunami amplification on that specific site.

Description of the Input Models

In this section we present the source models used to simulate the tsunami across the Indian Ocean. Models A and B depict first-order features of the 2004 source: even though they do not provide accurate description of the slip along the fault, they allow a comparison between a slightly heterogeneous (model A) and a homogeneous model (model B), with a refinement similar to other models used for trans-oceanic modeling (Titov *et al.*, 2005). Model C consists of a homogeneous source located in the 1833 epicentral area.

Model A

Earthquake model A relies on the results available from geodetic and seismological inversions of the 2004 rupture, that display many common features, such as increased slip around latitude 4° N–5° N, near 6° N and farther northward at about 10° N (Ammon *et al.*, 2005; Guilbert *et al.*, 2005; Vigny *et al.*, 2005; Subarya *et al.*, 2006; Chlieh *et al.*, 2007). Model A consists of six 130-km-wide subfaults, that dip from 12° to 15° from south to north, and that are associated with slips ranging from 3 m for the terminal subfaults 1 and 6, to 16 m for the subfault 4 located near 5° N (Table 1), yielding a total seismic moment of 6.76×10^{22} N m (or M_w 9.16). Model A does not aim at accurately imaging the rupture, as this was not the goal. The gradual tsunami triggering during the 9-min earthquake rupture duration could also contribute to modification of and interference between tsunami waves, at least in the near field. However model A reflects the high-energy release at 5° N and 8° N, characterized for these latitudes by an initial surface uplift reaching 3 m and more together with a subsidence well pronounced (Fig. 4), in good agreement with Global Positioning System (GPS) observations and models (e.g., Chlieh *et al.*, 2007).

Model B

Model B approximates the 2004 rupture by using the same slab geometry as in model A but with a homogeneous

Table 1
Parameters of the Subfaults Used for Model A

Subfault	Longitude ° E (Subfault Center)	Latitude ° N (Subfault Center)	Strike, Dip, Rake (°)	Length (km)	Slip (m) (Model A)	Slip (m) (Model B)
1	92.9	13.0	10, 15, 100	150	3	8.5
2	92.8	10.3	359, 14, 98	450	5	8.5
3	93.1	7.3	345, 13, 95	240	12	8.5
4	93.75	5.4	337, 12, 92	200	16	8.5
5	94.5	3.8	325, 12, 92	200	12	8.5
6	95.6	2.9	300, 12, 92	120	3	8.5

The central depth is 20 km, the fault width is 130 km throughout the rupture, and the rigidity is fixed to 45×10^9 N/m^2. This model yields a total seismic moment of 6.76×10^{22} N m, or a magnitude M_w 9.16.

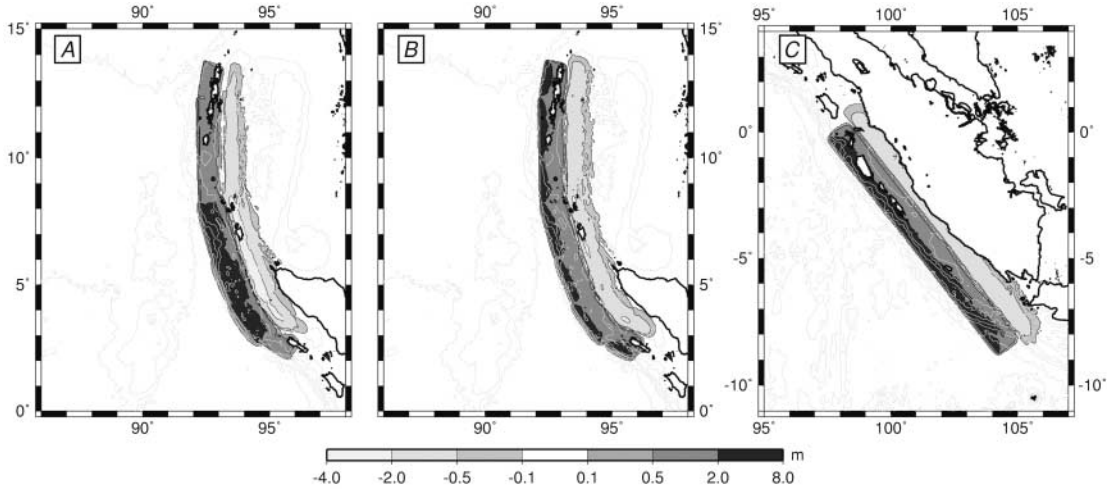

Figure 4. Ocean bottom coseismic deformation for models A, B, and C. Initial surface deformations range from −2.9 m to 7.3 m for model A, from −2.7 to 4.1 m for model B, and from −1.8 m to 4.3 m for model C. Bathymetric contour interval is 1000 m.

slip throughout the rupture, yielding the same seismic moment 6.76×10^{22} N m (or M_w 9.16), with a uniform fault slip amounting to 8.5 m. This model allows a comparison in the far field between slightly heterogeneous and homogeneous tsunami sources. The initial surface displacement reaches 2 m and more along the latitudinal extent of the rupture.

Model C

Finally we are also interested in providing some elements of tsunami hazard assessment for a source located southward, in a region where no large rupture has occurred since 1833 (Newcomb and McCann, 1987), and where stress triggering due to the 2004 and 2005 ruptures may have increased the probability for the next ruptures to the south (Nalbant *et al.*, 2005). This event should certainly trigger a transoceanic tsunami that could have an impact on many coastals areas in the Indian Ocean, as the 1833 earthquake most probably did (Estridge, 1883). The model C (Table 2) is homogeneous and extends over a presumably larger area than the 1833 rupture (Zachariasen *et al.*, 1999), at least southward toward the Sunda Strait, whereas its northern termination almost coincides with the southern extremity of the March 2005 rupture. The source characteristics are the same as in model B, with M_w 9.16.

Comparison of Models A and B with 2004 Altimetry Data

Although this study does not aim to precisely describing the source, the tsunami effect of models A and B has been compared with the altimetry data gathered 2 hours after the earthquake on satellites Topex-Poseidon and Jason (Ablain *et al.,* in press), which express the outstanding character of the Indian Ocean tsunami (Fig. 5). These records indeed reveal extreme peak-to-trough amplitudes of the wavefront that reach more than 1 m, to be compared with the signal identified on ERS1 in the 1990s for the Nicaragua earthquake, which hardly emerged from the background noise level (Okal *et al.*, 1999). In 2004, even though the mesoscale signal is not properly accounted for, the wavefront clearly

Table 2
Parameters of the Source (Model C) Used to Propagate a Tsunami from the 1833 Epicentral Region

Longitude ° E (Subfault Center)	Latitude ° N (Subfault Center)	Slip (m)	Strike, Dip, Rake (°)
101.4	−4.1	8.9	322, 14, 90

The central depth is 20 km, the fault width is 140 km, and length is 1200 km throughout the rupture, and the rigidity is fixed to 45×10^9 N/m^2. This model yields a total seismic moment of 6.76×10^{22} N m, or a magnitude M_w 9.16.

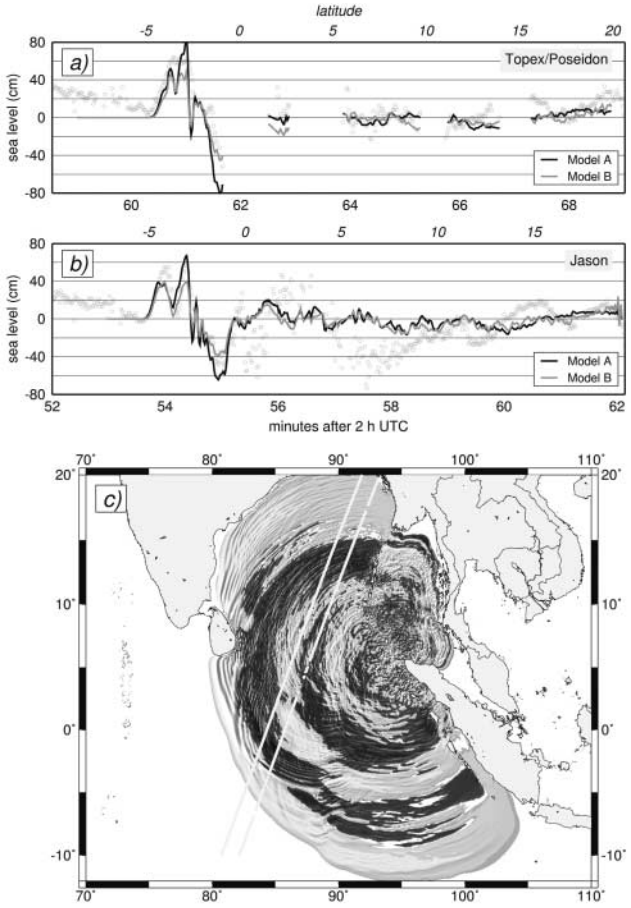

Figure 5. (a, b) Comparison of models A and B with altimetry signals. (c) Computed free surface after 2 hours of propagation (model A) is displayed with positive (negative) signal in light (dark) grey. Satellite tracks are also shown (Jason is the easternmost track). Similar previous and next surfaces (about 2 h after the earthquake) have been sampled at 20-sec intervals to account for the almost 10-min transit of each satellite in a and b.

appears as well as the following waves, especially on Jason data.

The free sea surfaces computed at 20-sec intervals have been sampled along the satellite tracks for corresponding time intervals, thus taking into account the almost 10-min transit of each satellite. The wavefront observed on both platforms Jason and Topex around 3–4° S is rather well fit while the more detailed Jason signal exhibits wave features extending between latitudes 0° and 15° N, that are not completely explained either by model A or model B. These central wave trains may reflect dispersive waves that are not accounted for in our computations. However similar non-dispersive computations with kinematic triggering of the tsunami manage to fit these central tsunami waves (Sladen and Hébert, 2005).

The snapshot of the sea surface after 2 hours of propagation (Fig. 5, bottom) shows that the northernmost computed wavefront is north to 20° N, probably rather in advance of the actual wavefront. The 9-min rupture propagation may partly explain the difference. Thus our wavefront fit to the north is rather poor, even though the northward transit of the satellite acts in the same direction and with the same duration as the earthquake rupture does: our analysis of the data actually considers the satellite transit time.

To summarize, neither model A nor B properly fits detailed features of the tsunami wave trains in the near and intermediate field. Notwithstanding computed amplitudes larger than observed ones (especially for second peak), both models A and B explain reasonably well the first waveform.

Also note that we may encounter some difficulties in studying with models A and B late arrivals in remote places as the ones noted in La Réunion, for instance, because they could come from wave trains observed between 0° and 15° N, due either to dispersive effects or to fine source characteristics that are not taken into account here.

Results for the 2004 Tsunami

At the Oceanic Scale

Although tsunami waves isotropically propagate across the ocean it is theoretically established that directivity effects influence the impact of a tsunami (Ben-Menahem and Rosenman, 1972; Okal, 1988). As also shown in numerical modeling, and illustrated by the maximum water heights computed over a complete tsunami propagation, the energy of a tsunami is preferentially directed perpendicular to the fault strike, defining regions at higher risk for a given rupture location (Hébert *et al.*, 2001). In 2004, the mean fault strike clearly defines higher risk areas, to the east (Sumatra, Thailand) and to the west (southern India, Sri Lanka, Maldives, and East Africa). The 1881 Andaman tsunami had a similar strike, though less extended than in 2004, and was similarly well observed at least in India, and must have struck Thailand too, even though the inferred source magnitude may not have exceeded 7.9 (Ortiz and Bilham, 2003).

The maximum water heights computed by our modeling in the Indian Ocean (Fig. 6) reveal these theoretically expected features, in addition to the wave trapping above shallow submarine ridges and plateaus that, in particular, led to trapping of wave energy over the Southwest Indian Ridge toward the Atlantic Ocean (Titov *et al.*, 2005). Both models A and B show the highest impact of the tsunami waves to-

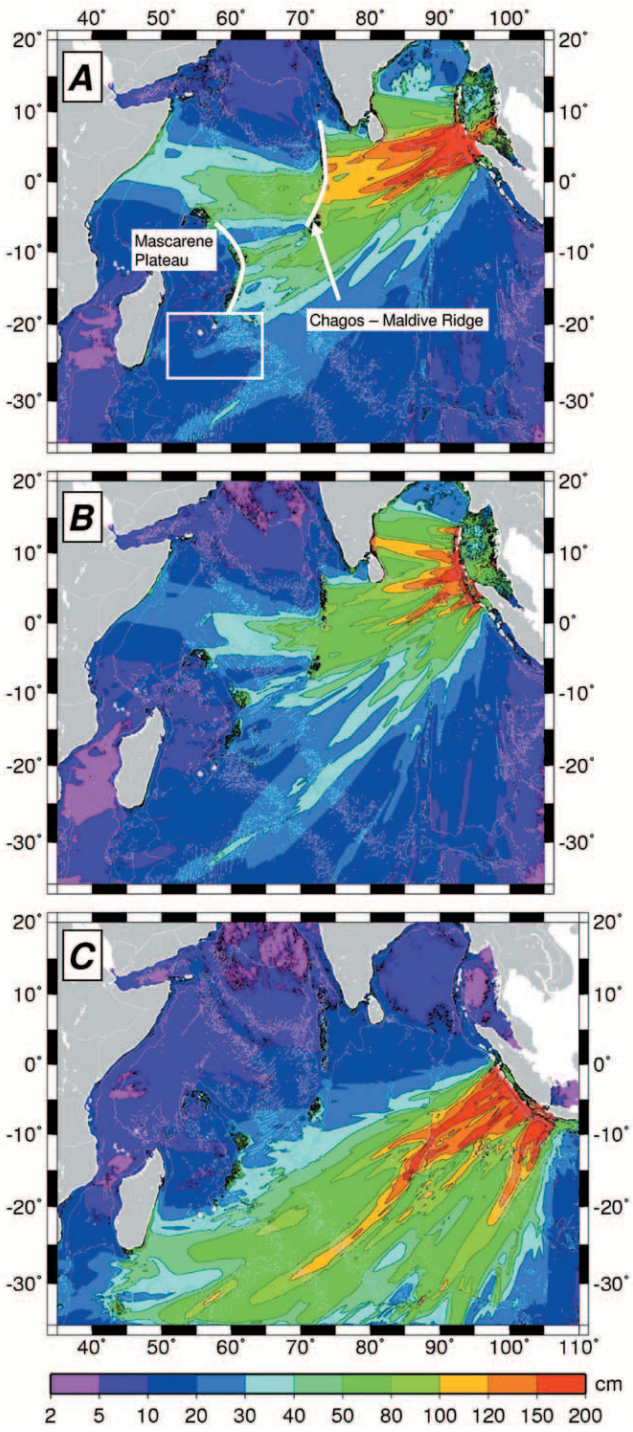

Figure 6. Computed maximum water heights after 12 hours of propagation in the Indian Ocean for models A, B, and C. The white rectangle indicates the Mascarene Islands region. Note the effect of oceanic features (ridges, plateaus) in lowering the tsunami impact.

ward Thailand, Sumatra, Sri Lanka, southern India, and East Africa. Note that the steep shallow submarine features also act as barriers able to reduce energy propagating farther, such as the Chagos-Maldive Ridge that seems to reduce the impact toward Somalia and Kenya: maximum heights of 100 to 120 cm observed to the east are stopped by the ridge. Similarly the Mascarene plateau also probably lowers the tsunami effect on the northern Madagascar region, where maximum heights of 10–30 cm (model A) or 5–20 cm (model B) are obtained compared with values 10 cm higher to the east of the Mascarene plateau.

These oceanic computations show that models A and B yield a different energy distribution in the ocean: the higher slip south of, and lower slip in the middle of model A directs greater energy toward the Maldives and less energy toward southern India, while the homogeneous model B leads to a high impact in southern India and especially Sri Lanka. The 5 to 10 m run-up values, actually observed in 2004 in southeastern India and Sri Lanka (Jayakumar *et al.*, 2005; Liu *et al.*, 2005) tend to indicate that the source requires high slip at latitudes close to 10° N, a feature that is not strictly respected in either model A or B, but that probably plays a minor role for the model toward the Mascarene.

Impact in the Mascarene

The Mascarene region is not directly located in the maximum lobe of expected energy because of its rather southern location with respect to the source. However the Mascarene islands lie in the southern part of the Mascarene Plateau and thus are not strictly in its "shadow." Although the computed tsunami waves arriving in the Mascarene Islands are not among the highest in the Indian Ocean, the maximum wave heights computed in the region range from 5 to 20 cm (model B) to 10 to 30 cm (model A). These different oceanic computed impacts are probably best accounted for by the different coseismic slip values considered in model A or B near 3°–5° N.

The computed tsunami waves first reached Rodrigues after 5 h 40 m of propagation, then Mauritius after 6 h 30 m, and La Réunion after 6 h 50 m (Fig. 7). For each island constructive interference of waves on the leeward direction of the arrival are probable, causing a possible increased impact on the southwestern side of Rodrigues, on the northwestern coast of Mauritius and on the western coast of La Réunion (Fig. 7). This tsunami wave trapping is frequently observed in computations and may explain amplifications in sites not exposed directly to the tsunami wavefront (Yeh *et al.*, 1994; Piatanesi and Tinti, 1998; Alasset *et al.*, 2006). The local site conditions then attenuate or amplify these arrival conditions, as in Rodrigues where a well-developed lagoon on the western coast could have decreased the interference effect (Okal *et al.*, 2006c). In La Réunion where the coral reef is only very localized south to Saint-Gilles, the observed run-up heights are actually higher on the western coastline (Okal *et al.*, 2006c).

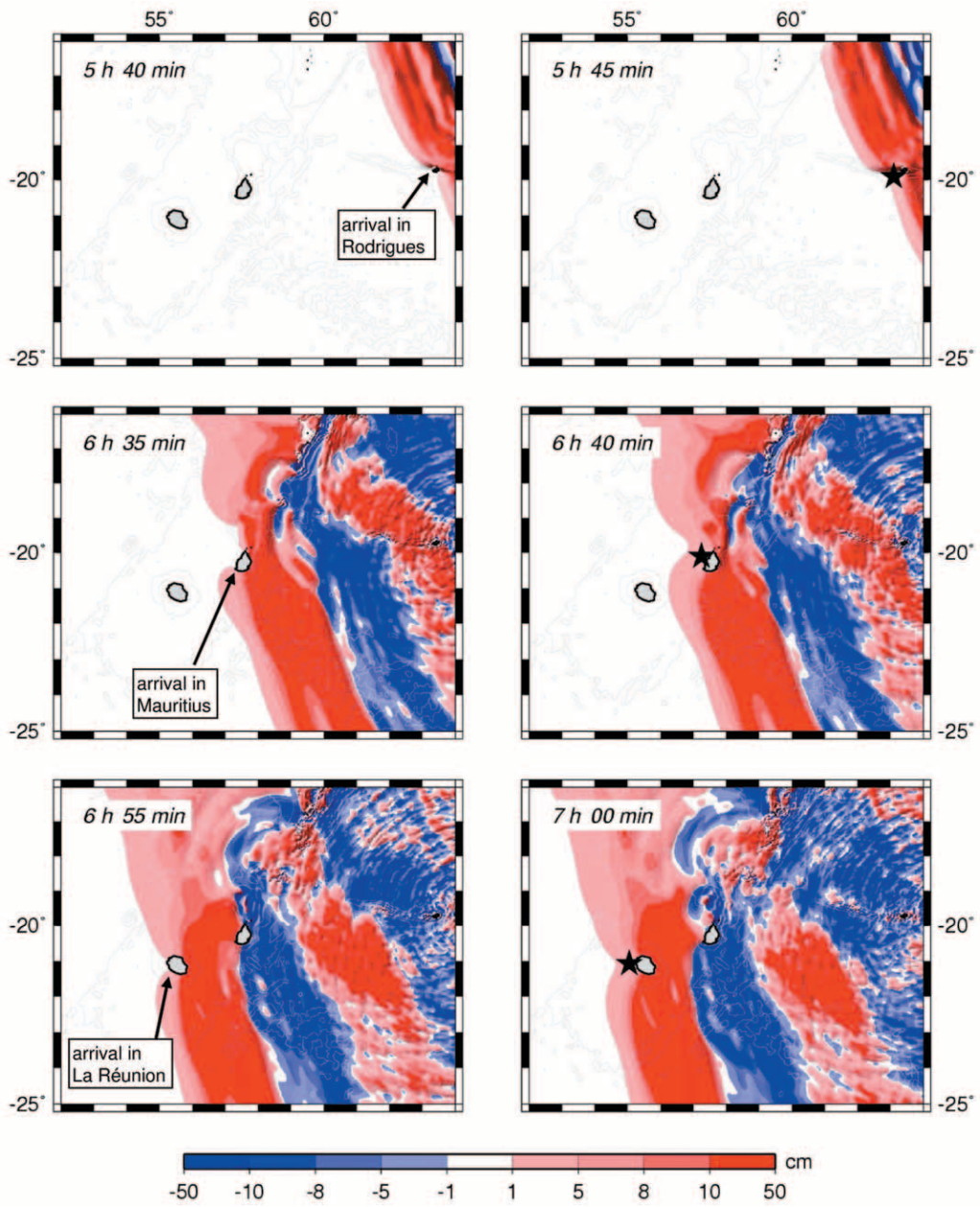

Figure 7. Wave arrival and trapping around the Mascarene Islands. The black stars denote the places where constructive interferences may have amplified the tsunami waves, before shallow coastal amplifying features (e.g., lagoon in Rodrigues). Bathymetric contour interval is 1500 m.

Impact in the Harbors in La Réunion

Synthetic computed tide gauges have been compared with the signals observed in the western basin of La Pointe des Galets (Fig. 8). For model A as for model B the arrival time is well fit when taking an origin time of 0 h 58 m 50 s UTC, which primarily reflects the triggering of the tsunami by the southernmost extremity of the fault. The corresponding source subfault also seems to be, along the tsunami travel path, the closest to the Mascarene Islands: the first tsunami arrivals therefore probably originate in the triggering of the tsunami near 3° N.

The computed sea level variations are discussed with respect to the observed signal (Fig. 8). At first sight, we observe that the waveforms are well fit at least for the first 60 to 90 min of signal, as is often the case in tsunami numerical studies: modeled waveforms are usually less reliable in the subsequent hours when numerical dispersion is enhanced. However, even in the first 90 min after the arrival,

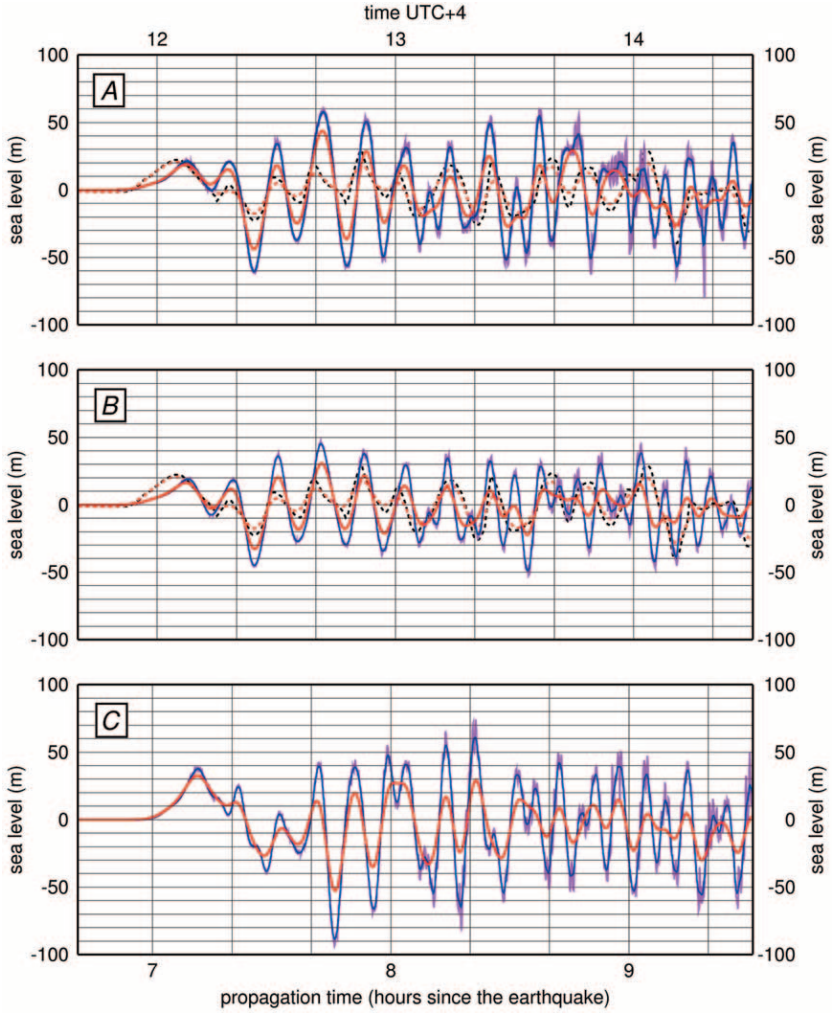

Figure 8. Synthetic tide gauges computed in the harbor of La Pointe des Galets (western basin) for models A, B, and C, displayed with the rough signal (pink), 1-min filtered (blue), and 10-min filtered signal (red). The 2004 observed (black dashed line) and 10-min filtered (red dashed line) tide gauge signal is compared with models A and B. The 1883-like model (C) is displayed as a function of equivalent propagation time since the earthquake.

we note that the amplitudes computed with both models A and B tend to be significantly larger than the 2004 observed signal, even though discrepancies are smaller for model B.

Note that more realistic source models now available from tsunami (Sladen and Hébert, 2005; Fujii and Satake, 2007; Piatanesi and Lorito, 2007) or seismological or geodetic studies (e.g., Ammon *et al.*, 2005; Subarya *et al.*, 2006) imply a fault slip much larger than the ones considered here, hence a higher tsunamigenic seafloor elevation, but spread over a rather small surface. The use of such models could notably increase our computed impact in La Réunion, stressing that our numerical modeling overestimates actual observations. This trend has already been observed in other areas (Balearic Islands in 2003; see Alasset *et al.*, 2006), and underlines the need for tsunami models to incorporate dissipation processes such as bottom friction and to better control possible numerical dispersion. Physical dispersion needs also to be tested further.

Another reason for the discrepancies may also come from the poorly known instrumental response. Indeed the real tide gauge provides a low-frequency signal compared with the high-frequency computed waveform that contains more information, including numerical noise. Most of the tide gauge observations are either naturally filtered (saturation, buoy blocked), or, for modern instruments, sampled at intervals of 1 min at least. For this analog tide gauge from La Réunion, the digitized signal is sampled at a better rate than 1 point/min, but this old instrument may not have recorded all fine oscillations. As an illustration, the 10-min filtered computed waveforms (Fig. 8, red line) are compared with the 10-min filtered observed signal (red dashed line), which is very close to the original signal. The filtered signal could perfectly mimic a real tide gauge that is not perfectly responding to sea level variations, or that is cut off at a long period (Alasset *et al.*, 2006). We can also mention that the clipped amplitudes in the original paper record (Fig. 2a) unlikely contribute to the difference between computed and observed signals because the missing peaks do not exceed the digitized ones by more than 5 cm.

Finally both models A and B overestimate observations, although model B is closer to the actual signal. The comparison with altimetry already showed that the models yielded amplitudes too large in the deep ocean. Because the total seismic moment is the same for models A and B, the

slip heterogeneities, or, at least, the fault-slip value contributing the most to the arrival in the remote islands, appear to or may influence the tsunami impact. This also confirms that remote tide gauges, considered within their error levels, can reasonably be used to constrain the source parameters of tsunamigenic earthquakes. They can even be inverted for this purpose, provided they are spatially well located around the source region (e.g., Tanioka and Satake, 2001; Fujii and Satake, 2007; Piatanesi and Lorito, 2007).

The computed maximum water heights and the run-up reached during the two hours following the first arrivals, in the three harbors studied, reveal values close to the actual observations. In the western basin (Fig. 9, top), 0.5–1 m (model A) or 0.3–0.5 m (model B) water heights are obtained in the basin, whereas the eastern harbor (Fig. 9, middle) is characterized by 1.5 (model B) to 2.5 m (model A). The 2.7-m-high run-up observed here (see Fig. 3 for location) is thus better explained with model A in the eastern basin.

The calculated impact is the largest in Saint-Gilles (Fig. 9, bottom), where offshore values exceed 2.5 m over a large area offshore. The onland computed run-up heights are much larger than the reported 2.4-m value, casting some doubt on our modeling here (especially because of topographic uncertainties) or indicating that the observed run-up on the beach underestimates the actual impact, but this was not suggested from witnesses.

Results for a 1833-Similar Source

At the Oceanic Scale

The maximum water heights reached in the Indian Ocean for the 1833-like source (Fig. 6c) display the same level of tsunami energy spread over the ocean as in 2004, except that the natural barriers lowering the impact are fewer, except for the NinetyEast Ridge that slightly reduces the values. At first sight this tsunami is as gigantic as in 2004 but the exposed emerged coastlines are less numerous, except for several austral islands in the southern Indian Ocean, and possibly Antarctica and Australia. In India or Sri Lanka, the maximum water heights off the coasts, in deep water, are locally ten times smaller than the values obtained for models A and B.

For the Mascarene Islands however, the impact seems to be larger, because the computed maximum water heights reach 20 to 50 cm, thus almost twice the 2004 level.

Detailed Impact

The synthetic tide gauges (Fig. 8, bottom) exhibit larger values than in 2004 (models A and B) with peak-to-trough amplitudes reaching more than 150 cm (unfiltered) or almost 100 cm (10-min filtered). Therefore the impact in the western harbor of La Pointe des Galets is almost one and a half the impact in 2004, yielding a maximum height of 80 cm when the 2004 models yielded 50–60 cm. The wave arrivals are slightly later than in 2004 with a 5- to 10-min delay.

The computed maximum water heights (Fig. 10) reach almost 1 m in La Pointe des Galets (western basin) and more than 2 m in the eastern harbor, they exceed 3 m in Saint-Gilles, in agreement with an offshore mean impact 1.5 to 2 times greater than the 2004 models. Also note that the relative results between the two basins of La Pointe des Galets are different for model C, with the western harbor relatively more struck in model C than in models A and B. This result reminds us that the final relative amplitudes around an island depend on the arrival azimuth, and, for La Réunion, that the western harbor is relatively more exposed for a 1833-like source than for the 2004 source, whereas the impact in the eastern harbor is hardly exceeding the 2004 impact. As for Saint-Gilles the computed impact is anyway much larger, almost twice, than in 2004.

Discussion

Impact of the 2004 Tsunami

Our numerical modeling suggests that models A and B are reasonable approximations of the earthquake source that appear to explain altimetry data and remote observations. These first-order source models, as well as the refined models now available, should now be tested using improved numerical modeling able to take into account kinematic tsunami triggering and dispersive waves.

Our results confirm first-order impact on the eastern Mascarene Islands with a protecting lagoon that probably reduced the effect in western Rodrigues. On these islands however, detailed computations have not yet been achieved, because they would require another set of bathymetric and topographic data that are still to be realized. These modelings would allow the comparison with the results obtained for La Réunion. On that point we note that the 2004 tide gauge data seem to be quite representative for a lower tsunami impact in the western harbor than in the eastern harbor, as is confirmed by the computations. The offshore computed maximum water heights are not really different off both basins (Fig. 9), but the contrasting basin exposures and dimensions, or the different harbor mouth configurations, may explain the impact and resonance in each basin, respectively.

On the contrary the effect on Saint-Gilles appears to be the highest, and observations did not mention a more important tsunami effect here. This may be due to overestimation in the computational result, although we have noted that the wider submarine shallow shelf off Saint-Gilles creates convenient conditions to amplify tsunami waves: local coastal features therefore may have lowered the impact onshore.

Origin of the Late Disturbances

The late harbor amplifications, or disturbances, that led to the breaking of moorings of a container ship in La Pointe des Galets (eastern basin) have to be discussed. Both moor-

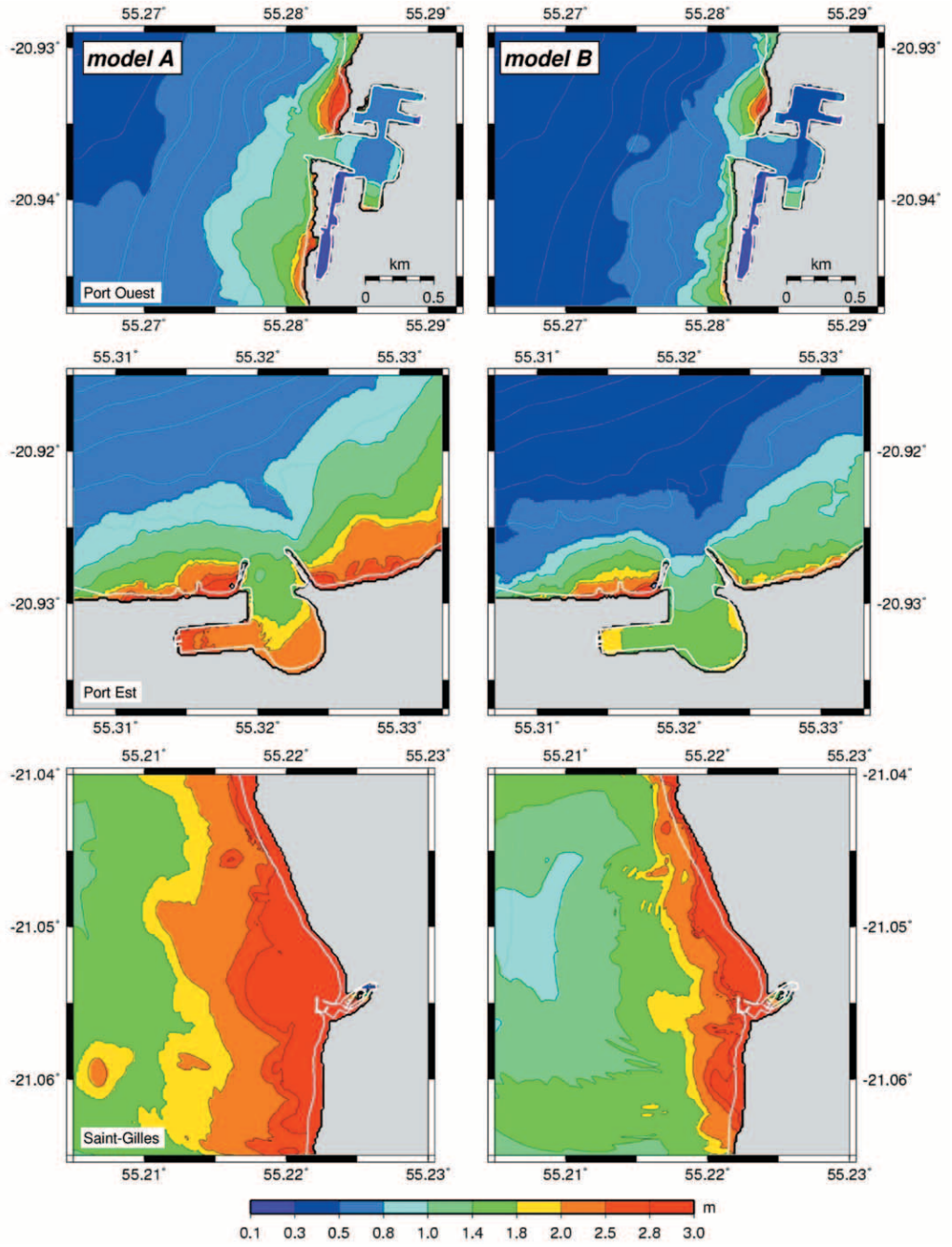

Figure 9. Maximum water heights reached in the three studied sites of La Réunion, displayed for the first 2 hours after the wave arrivals. Run-up values on land are displayed up to 3 m height, since the higher topographic features are poorly constrained. In Saint-Gilles, the run-ups actually computed exceed 4 m.

ing breaks occurred between 10 h 30 m and 11 h, and then around 13 h 30 m of propagation time.

For these times of propagation, reflected waves coming back from Madagascar and from a secondary reflection on Sumatra seem also to reach the Mascarene area (Fig. 11). These reflections are evidenced for both source models A and B, indicating that they are quite robust with respect to fault-slip heterogeneities; our nondispersive model emphasizes well this kind of oceanic reflection. Numerous reflections have also been observed in hydroacoustic data (Hanson *et al.*, 2007). Some of these dispersed wave trains arrive during at least 20 hr following the earthquake. The reflection on Madagascar, however, is not observed on those data where it could be present in Cocos (at least 16 h after the earthquake deduced from our modeling) or Crozet (about 13 h after the earthquake) (see figure 15 in Hanson *et al.*,

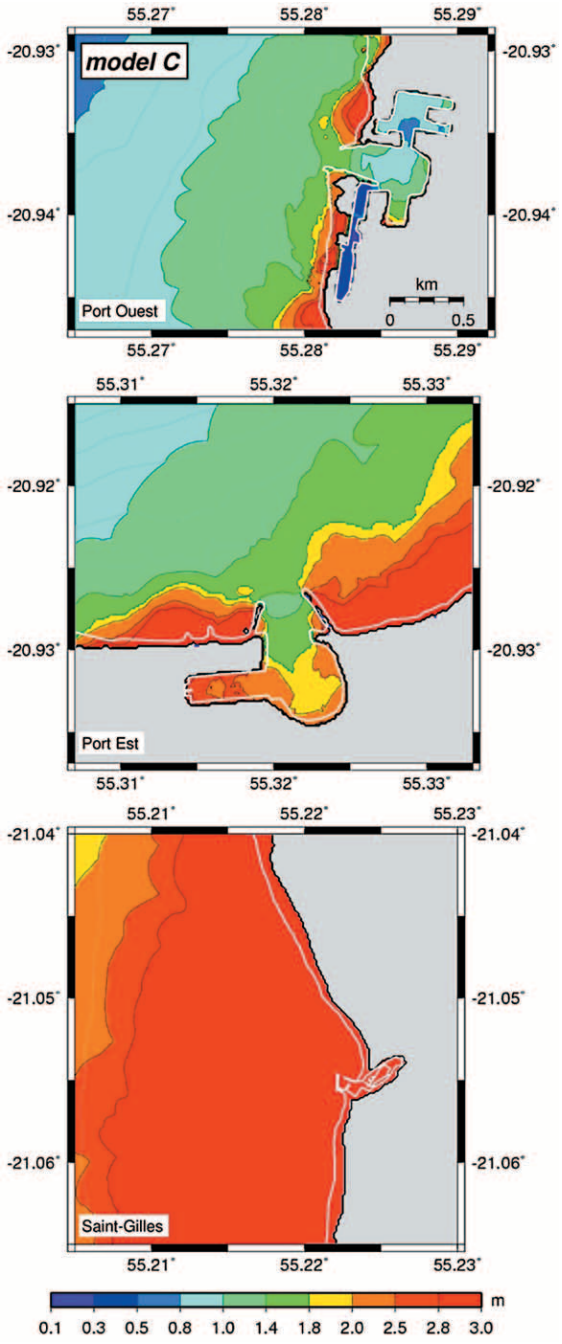

Figure 10. Maximum water heights reached in the three studied sites of La Réunion, displayed for the first 2 hours after the wave arrivals, for the 1833-like model C.

2007). The secondary reflection is obviously more difficult to identify. A second wave train arrival clearly observable on the spectral analysis of the tide gauge data in La Pointe des Galets (Rabinovich and Thomson, 2007) could, however, well correspond to this secondary distant reflection.

We failed to identify energetic signal arriving at these hours off the harbors of La Pointe des Galets, because in this long-lasting computation numerical dispersion becomes too important. Off Saint-Gilles, however, the computed wave trains exhibit several significant interesting late waveforms that may correspond to the arrivals of reflected signals (Fig. 12). The corresponding times do not perfectly match the time when moorings broke, while a reflection coming from Madagascar should strike the western coast of La Réunion almost at the same time, or with differences of 10–15 min at most. But we note that late arrivals of tsunami energy are evidenced in numerical modeling, and are almost unclear in the tide gauge available (Fig. 2). Finally the break of moorings could also be due to harbor resonances in response to the late arrivals, whatever their cause. The continuously dispersed wave trains observed on hydroacoustic signals may also have contributed to provoke these disturbances, creating possible complex interactions during the development of harbor resonances.

What's Next?

Finally an expected rupture south of the 2004 and 2005 ruptures coinciding and even possibly exceeding the 1883 rupture would create a great transoceanic tsunami, although exposed inhabited coastlines may be fewer. For the Mascarene Islands however, the impact is expected to be larger, also indicating that a smaller rupture in the source area could trigger a 2004-like impact in La Réunion: detailed hazard assessment should therefore be performed for the Mascarene Islands.

Our results for the three models A, B, and C are encouraging because we succeed in reproducing in our numerical results many features of the tsunami and feel more confident in applying similar methods for hazard assessment elsewhere (e.g., French Polynesia; Hébert *et al.*, 2001). However, the 2004 Indian Ocean tsunami also provides an outstanding opportunity to test numerical modeling, and this study is only preliminary in this respect.

Indeed, the quality and number of the data gathered after the event invite us to consider refined modeling in the near and in the far field. In addition to the treatment of the dispersive waves that should at least be tested and compared with these modern data, local responses of coastlines can now be finely tuned, and could for instance lead us to precisely define bottom friction parameters to account for features such as lagoon, reefs, or mangroves. And even though the rupture kinematics probably weakly influence the far-field impact, taking into account the slip history will also be worth testing to study fine responses in the near field.

Conclusion

We have simulated the 2004 tsunami using two different source models, accounting for first-order source characteristics and allowing us to test the role of slip heterogeneities. The computed tsunami waveforms are in good agreement with the tide gauge data observed in La Réunion, where nested bathymetric grids with increasing resolution allowed

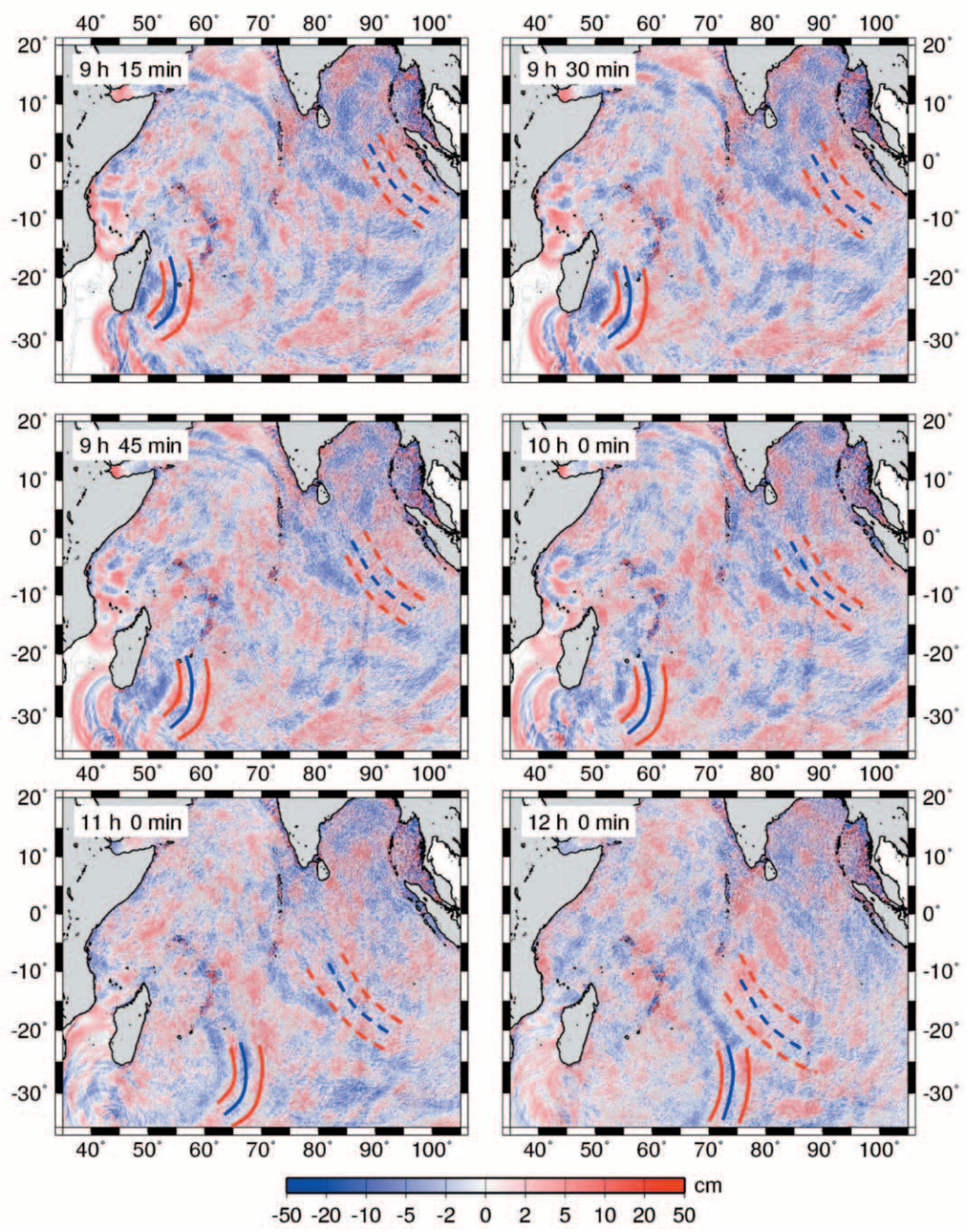

Figure 11. Snapshots of the tsunami wave field (model A) showing several reflections on coastlines or shallow oceanic features (ridge, plateaus). A reflection on Madagascar (solid red and blue lines) is evidenced from 9 hours of propagation, and propagates back toward the Mascarene Islands. A more questionable secondary reflection on Sumatra also occurs (dashed red and blue lines), coming back from a primary reflection on Sri Lanka and Maldives.

computation of the tsunami impact in harbors. The computed amplitudes are too large, however, suggesting a source too energetic for the subfault contributing to the far-field effect, and stressing the need to test dissipation in numerical models. A main outcome is that fault heterogeneities, for these gigantic subduction earthquakes, are able to influence the tsunami impact in remote places. Finally, the use of a 1833-like source (model C) indicates an impact even larger for the harbors studied in La Réunion, but the former result also stresses that further detailed studies using more heterogenous faults are required to properly assess the impact for this expected tsunami.

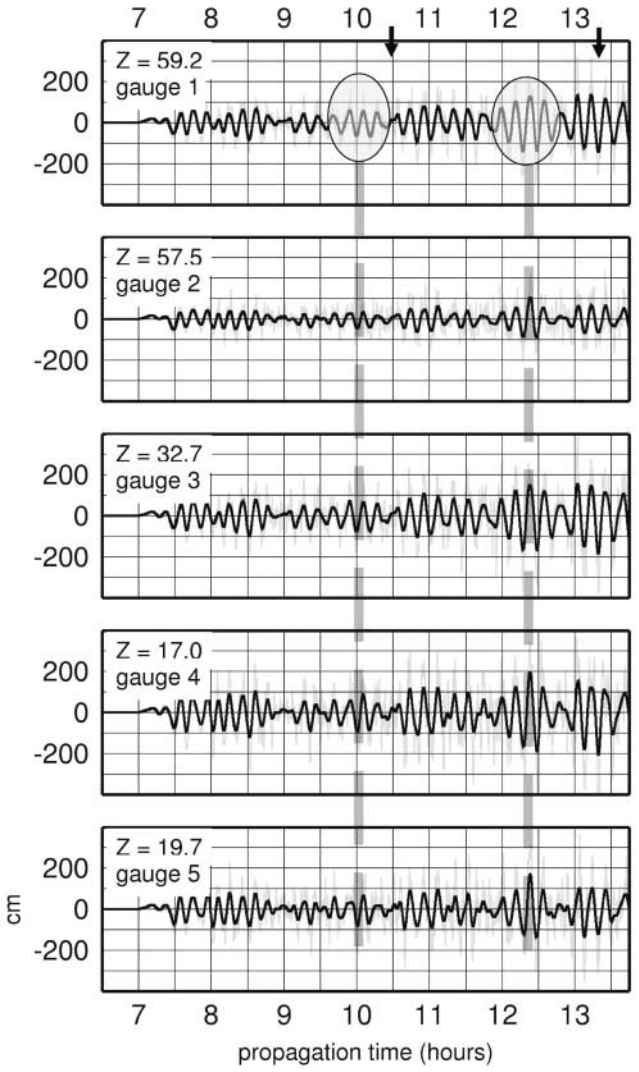

Figure 12. Sea level variations computed off Saint-Gilles, displayed as the rough computed signal (grey line) and the 10-min filtered signal (black line) (location of gauges on Fig. 3). Black arrows indicate the approximate hours when the moorings of the container ship were broken in the eastern harbor, whereas grey shaded areas indicate wave trains possibly related to distant reflections.

Acknowledgments

We thank the Direction Départementale de l'Equipement (DDE) from La Réunion for providing us with the tide gauge record in the harbor of La Pointe des Galets and for their preprocessing of the data. The SHOM (French Hydrographic Service) also provided some useful technical comments on the tide gauge material. The processing of altimetry data has benefited from many useful and ongoing discussions with M. Ablain (CLS, Space Oceanography Division). Constructive comments made by K. Satake and two anonymous reviewers helped improve the clarity of the manuscript. This article also benefited from support of CEA/DASE and French Agence Nationale de la Recherche through grant CATTELL TSUMOD ANR-05-CATT-016-01. Figures were created with Generic Mapping Tools (Wessel and Smith, 1998).

References

Ablain, M., J. Dorandeu, P.-Y. Le Traon, and A. Sladen (2006). High resolution altimetry reveals new characteristics of the December 2004 Indian Ocean tsunami, *Geophys. Res. Lett.* (in press).

Alasset, P. J., H. Hébert, V. Calbini, S. Maouche, and M. Meghraoui (2006). The tsunami induced by the 2003 Zemmouri earthquake (Mw = 6.9, Algeria): modelling and results, *Geophys. J. Int.* **166,** 213–226, doi 10.1111/j.1365-246×.2006.02912.x.

Ammon, C. J., C. J. Ammon, C. Ji, H. Thio, D. Robinson, S. Ni, V. Hjorleifsdottir, H. Kanamori, T. Lay, S. Das, D. Helmberger, G. Ichinose, J. Polet, and D. Wald (2005). Rupture process of the 2004 Sumatra-Andaman earthquake, *Science* **308,** 1133–1139.

Ben-Menahem, A., and M. Rosenman (1972). Amplitude patterns of tsunami waves from submarine earthquakes, *J. Geophys. Res.* **77,** 3097–3128.

Chlieh, M., J.-P. Avouac, V. Hjorleifsdottir, T.-R. A. Song, C. Ji, K Sieh, A. Sladen, H. Hebert, L. Prawirodirdjo, Y. Bock, and J. Galetzka (2007). Coseismic Slip and Afterslip of the Great (Mw9.15) Sumatra-Andaman Earthquake of 2004, *Bull. Seism. Soc. Am.* **97,** no. 1A, S152–S173.

Chlieh, M., J.-B. de Chabalier, J.-C. Ruegg, R. Armijo, R. Dmowska, J. Campos, and K L. Feigl (2004). Crustal deformation and fault slip during the seismic cycle in the North Chile subduction zone, from GPS and InSAR observations, *Geophys. J. Int.* **158,** 695–711.

Delouis, B., T. Monfret, L. Dorbath, M. Pardo, L. Rivera, D. Comte, H. Haessler, J. P. Caminade, L. Ponce, E. Kausel, and A. Cisternas (1997). The Mw = 8.0 Antofagasta (Northern Chile) earthquake of 30 July 1995: a precursor to the end of the large gap of 1877, *Bull. Seism. Soc. Am.* **87,** 427–445.

Duncan, R. A. (1981). Hotspots in the southern oceans—an absolute frame of reference for motion of the Gondwana continents, *Tectonophysics* **74,** 29–42.

Estridge, H. W. (1883). The recent phenomena, *The Mercantile Record and Commercial Gazette*, 5th October 1883, 115–116.

Fujii, Y., and K. Satake (2007). Tsunami source of the 2004 Sumatra-Andaman earthquake inferred from tide gauge and satellite data, *Bull. Seism. Soc. Am.* **97,** no. 1A, S192–S207.

Gower, J. (2005). Jason-1 detects the December 26 2004 tsunami, *EOS Trans. AGU* **86,** no. 4, 37–38.

Guilbert, J., J. Vergoz, E. Schisselé, A. Roueff, and Y. Cansi (2005). Use of hydroacoustic and seismic arrays to observe rupture propagation and source extent of the Mw = 9.0 Sumatra earthquake, *Geophys. Res. Lett.* **32,** L15310, doi 10.1029/2005GL022966.

Hanson, J. A., and J. R. Bowman (2005). Dispersive and reflected tsunami signals from the 2004 Indian Ocean tsunami observed on hydrophones and seismic stations, *Geophys. Res. Lett.* **32,** doi 10.1029/2005 GL023783.

Hanson, J. A., C. Reasoner, and J. R. Bowman (2007). High frequency tsunami signals of the great Indonesian earthquakes of 26 December 2004 and 28 March 2005, *Bull. Seism. Soc. Am.* **97,** no. 1A, S232–S248.

Hébert, H., P. Heinrich, F. Schindelé, and A. Piatanesi (2001). Far-field simulation of tsunami propagation in the Pacific Ocean: impact on the Marquesas Islands (French Polynesia), *J. Geophys. Res.* **106,** no. C5, 9161–9177.

Hébert, H., F. Schindelé, Y. Altinok, B. Alpar, and C. Gazogliu (2005). Tsunami hazard in the Marmara Sea (Turkey): a numerical approach to discuss active faulting and impact on the Istanbul coastal areas, *Mar. Geol.* **215,** 23–43.

Heinrich, P., F. Schindelé, S. Guibourg, and P. Ihmlé (1998). Modeling of the February 1996 Peruvian tsunami, *Geophys. Res. Lett.* **25,** 2687–2690.

Jayakumar, S., D. Ilangovan, K. A. Naik, R. Gowthaman, G. Tirodkar, G. N. Naik, P. Ganeshan, R. M. Murali, G. S. Michael, M. V. Ramana, and G. C. Bhattacharya (2005). Run-up and inundation limits along

southeast coast of India during the 26 December 2004 Indian Ocean tsunami, *Curr. Sci. India* **88,** no. 11, 1741–1743.

Kanamori, H., and D. Anderson (1975). Theoretical basis of some empirical relations in seismology, *Bull. Seism. Soc. Am.* **65,** 1073–1095.

Lay, T., H. Kanamori, C. J. Ammon, M. Nettles, S. N. Ward, R. Aster, S. L. Beck, S. L. Bilek, M. R. Brudzinski, R. Butler, H. R. DeShon, G. Ekström, K. Satake, and S. Sipkin (2005). The great Sumatra-Andaman earthquake of 26 December 2004, *Science* **308,** 1127–1132.

Le Pichon, A., P. Herry, P. Mialle, J. Vergoz, N. Brachet, M. Garcés, D. Drob, and L. Ceranna (2005). Infrasound associated with 2004-2005 large Sumatra earthquakes and tsunami, *Geophys. Res. Lett.* **32,** L19802, doi 10.1029/2005GL023893.

Liu, P. L.-F., P. Lynett, H. Fernando, B. E. Jaffe, H. Fritz, B. Higman, R. Morton, J. Goff, and C. Synolakis (2005). Observations by the International Tsunami Survey Team in Sri Lanka, *Science* **308,** 1595.

Merrifield, M. A., Y. L. Firing, T. Aarup, W. Agricole, G. Brundrit, D. Chang-Seng, R. Farre, B. Kilonsky, W. Knight, L. Kong, C. Magori, P. Manurung, C. McCreery, W. Mitchell, S. Pillay, F. Schindele, F. Shillington, L. Testut, E. M. S. Wijeratne, P. Caldwell, J. Jardin, S. Nakahara, F.-Y. Porter, and N. Turetsky (2005). Tide gauge observations of the Indian Ocean tsunami, December 26, 2004, *Geophys. Res. Lett.* **32,** L09603, doi 10.1029/2005GL022610.

Morgan, W. J. (1981). Hotspot tracks and the opening of the Atlantic and Indian Oceans, in *The Sea*, C. Emiliani (Editor), Vol. 7, Wiley, New York, 443–487.

Nalbant, S. S., S. Steacy, K. Sieh, D. Natawidjaja, and J. McCloskey (2005). Earthquake risk on the Sunda trench, *Nature* **435,** 756–757.

Newcomb, K. R., and W. R. McCann (1987). Seismic history and seismotectonics of the Sunda arc, *J. Geophys. Res.* **92,** 421–439.

Okada, Y. (1985). Surface deformation due to shear and tensile faults in a half-space, *Bull. Seism. Soc. Am.* **75,** 1135–1154.

Okal, E. A. (1988). Seismic parameters controlling far-field tsunami amplitudes: a review, *Nat. Hazards* **1,** 67–96.

Okal, E. A., H. M. Fritz, R. Raveloson, G. Joelson, P. Pančošková, and G. Rambolamanana (2006a). Madagascar field survey after the December 2004 Indian Ocean tsunami, *Earthquake Spectra* **22,** S263–S283.

Okal, E. A., H. M. Fritz, C. E. Synolakis, P. E. Raad, Y. Al-Shijbi, and M. Al-Saifi (2006b). Oman field survey after the December 2004 Indian Ocean tsunami, *Earthquake Spectra* **22,** S203–S218.

Okal, E. A., A. Piatanesi, and P. Heinrich (1999). Tsunami detection by satellite altimetry, *J. Geophys. Res.* **104,** 599–615.

Okal, E. A., A. Sladen, and E. A.-S. Okal (2006c). Rodrigues, Mauritius, and Réunion Islands field survey after the December 2004 Indian Ocean tsunami, *Earthquake Spectra* **22,** S241–S261.

Ortiz, M., and R. Bilham (2003). Source area and rupture parameters of the 31 December 1881 Mw = 7.9 Car Nicobar earthquake estimated from tsunamis recorded in the Bay of Bengal, *J. Geophys. Res.* **108,** doi 10.1029/2002JB001941.

Piatanesi, A., and S. Lorito (2007). Rupture process of the 2004 Sumatra-Andaman earthquake from tsunami waveform inversion, *Bull. Seism. Soc. Am.* **97,** no. 1A, S223–S231.

Piatanesi, A., and S. Tinti (1998). Finite-element numerical simulations of tsunamis generated by earthquakes near a circular island, *Bull. Seism. Soc. Am.* **88,** 609–620.

Rabinovich, A. B., and R. E. Thomson (2007). The 26 December 2004 Sumatra tsunami: analysis of tide gauge data from the World Ocean. Part 1. Indian Ocean and South Africa, *Pure Appl. Geophys.* (in press).

Sladen, A., and H. Hébert (2005). Inversion of satellite altimetry data to recover the Sumatra 2004 earthquake slip distribution (abstract), *EOS Trans. AGU* **86,** no. 52 (Fall Meet. Suppl.), U22A-07.

Smith, W. H. F., and D. T. Sandwell (1997). Global seafloor topography from satellite altimetry and ship depth soundings, *Science* **277,** 1956–1962.

Stein, S., and E. A. Okal (2005). Size and speed of the Sumatra earthquake, *Nature* **434,** 581–582.

Subarya, C., M. Chlieh, L. Prawirodirdjo, J.-P. Avouac, Y. Bock, K. Sieh, A. J. Meltzner, D. H. Natawidjaja, and R. McCaffrey (2006). Plate-boundary deformation associated with the great Sumatra–Andaman earthquake, *Nature* **440,** 46–51.

Tanioka, Y., and K. Satake (2001). Detailed coseismic slip of the 1944 Tonankai earthquake estimated from tsunami waveforms, *Geophys. Res. Lett.* **28,** 1075–1078.

Titov, V., A. B. Rabinovich, H. O. Mofjeld, R. E. Thomson, and F. I. González (2005). The Global Reach of the 26 December 2004 Sumatra Tsunami, *Science* **309,** 2045–2048.

Vigny, C., W. J. F. Simons, S. Abu, R. Bamphenyu, C. Satirapod, N. Choosakul, C. Subarya, A. Socquet, K. Omar, H. Z. Abidin, and B. A. C. Ambrosius (2005). Insight into the 2004 Sumatra-Andaman earthquake from GPS measurements in southeast Asia, *Nature* **436,** 201–206.

Wessel, P., and W. H. F. Smith (1998). New, improved version of Generic Mapping Tools released, *EOS Trans. AGU* **79,** no. 47, 579.

Yeh, H., P. Liu, M. Briggs, and C. Synolakis (1994). Propagation and amplification of tsunamis at coastal boundaries, *Nature* **372,** 353–355.

Zachariasen, J., K. Sieh, F. W. Taylor, R. L. Edwards, and W. S. Hantoro (1999). Submergence and uplift associated with the giant 1833 Sumatran subduction earthquake: evidence from coral microatolls, *J. Geophys. Res.* **104,** 895–919.

Commissariat à l'Energie Atomique
Département Analyse, Surveillance, Environnement
BP12, 91680 Bruyères-le-Châtel, France

Manuscript received 9 January 2006.